Lab on a Chip

Cite this: *Lab Chip*, 2012, **12**, 2053–2059

www.rsc.org/loc

**PAPER**

# Capacitance-based droplet position estimator for digital microfluidic devices

**Miguel Angel Murran and Homayoun Najjaran***

***Received 13th December 2011, Accepted 7th March 2012***
**DOI: 10.1039/c2lc21241b**



Digital microfluidic (DMF) devices manipulate minuscule droplets through basic fluidic operations including droplet transport, mixing and splitting commonly known as the building blocks for complete laboratory analyses on a single device. A DMF device can house various chemical species and confine chemical reactions within the volume of a droplet much like a micro-reactor. The automation of fluidic protocols requires a feedback controller whose sensor is capable of locating droplets independent of liquid composition (or previous knowledge of liquid composition). In this research, we present an estimator that tracks the continuous displacement of a droplet between electrodes of a DMF device. The estimator uses a dimensionless ratio of two electrode capacitances to approximate the position of a droplet, even, in the domain between two adjacent electrodes. This droplet position estimator significantly enhances the control precision of liquid handling in DMF devices compared to that of the techniques reported in the literature. It captures the continuous displacement of a droplet; valuable information for a feedback controller to execute intricate fluidic protocols including droplet positioning between electrodes, droplet velocity and acceleration control. We propose a state estimator for tracking the continuous droplet displacement between two adjacent electrodes. The dimensionless nature of this estimator means that any droplet composition can be sensed. Thus, no calibration for each chemical species within a single DMF device is required. We present theoretical and experimental results that demonstrate the efficacy of the position estimator in approximating the position of the droplet in the interval between two electrodes.

## 1 Introduction

In recent years, there has been an increasing interest in miniaturizing sample volumes for laboratory analyses. The main advantages of volume reduction include shorter reaction time, higher sensitivity, as well as, reduced reagent consumption and waste production.[1] Traditionally, experimental analyses are executed in specialized laboratory equipment that is operated by highly trained personnel. Such laboratory equipment is typically sophisticated, immense, expensive, and high maintenance.

Digital microfluidic (DMF) systems thrive in the field of biotechnology with broad applications in cell analyses,[2,3] protein analyses,[4] DNA analyses,[5] and drug discovery.[6] The motivation behind building digital microfluidic devices is their re-programmability, portability, disposability and low power consumption.

A DMF system operates on micro-scale droplets over a planar surface. Complete experimental analyses are carried out in DMF devices through basic fluidic operations including droplet dispensing, moving, splitting, mixing and merging.[7] To date, several droplet actuation techniques have been proposed, including the use of chemical gradients,[8] electromechanics,[9–17] magnetic fields,[18] photoradiation,[19] surface acoustic waves,[20] and thermal gradients.[8,21] Of these droplet actuation mechanisms, electromechanics is the preferred liquid handling technique due to low power consumption and simple device fabrication.[22] With electromechanic actuation, droplets are manipulated over an array of electrodes by applying electrical signals to the individual electrodes. When an electrode is energized, electromechanical forces pull a neighbouring droplet towards the energized electrode. Thus, a discrete droplet displacement of approximately an electrode's width is achieved. Larger droplet displacements are achieved by sequentially energizing successive electrodes. The maximum droplet transfer rate or the frequency at which successive electrodes are energized is pre-determined experimentally.[15] This droplet control methodology assumes the droplet transferred completely over an energized electrode in the pre-calibrated actuation time before energizing the next electrode. This control methodology is referred to as an open loop control system because it is based on pre-calibrated operation conditions and lacks feedback information.

Open loop control systems have easy implementation and perform well under pre-calibrated system conditions with no feedback information. But, due to the lack of feedback information, the control cannot correct for disturbances that change the dynamics of the system. For example, surface imperfection, like dust particles, impede droplet motion to slow the transport of droplet to the adjacent electrode. This affects the

*School of Engineering, University of British Columbia, 3333 University Way Kelowna, BC, V1V 1V7, Canada. E-mail: h.najjaran@ubc.ca; Fax: +1 250 807 8713; Tel: +1 250 807 8713*

performance of the open loop controller because the electrical signals will continue to actuate the electrode while the droplet falls behind and does not follow the energized electrode. A closed loop (or feedback) controller uses feedback information to correct for random disturbances to the system. In a feedback controller for DMF devices, the controller has a mechanism for sensing that the droplet has properly transferred over the energized electrode before proceeding to energize the next electrode.

Shin *et al.*[23] implemented a feedback controller with visual relay information. The controller locates a droplet over an electrode by detecting circular objects within a circular boundary over an electrode. Then, driving signals are applied to the adjacent electrode and the process repeats. Visual feedback can be used to detect various droplet compositions, however, it requires high precision imaging equipment and high computational power for image processing.

Shih *et al.*[24] implemented a feedback controller system with an electronic sensor for AC electrical driving signals. The sensor is composed of a network of passive electrical components in series with the ground plate in a DMF device. The sensor draws power from an AC driving signal to produce a voltage feedback signal whose magnitude increases with increasing droplet footprint over the energized electrode. The controller compares the voltage feedback signal with a threshold voltage to determine whether the droplet has successfully transferred over the energized electrode before energizing the next electrode. This threshold voltage requires pre-calibration because it depends on the droplet electrical properties and frequency of the AC driving signal. This approach has practical implementation for droplet transport, however, we foresee limitations imposed by the voltage feedback signal that requires tuning the sensor impedance and calibrating the threshold voltage which depends on droplet electrical properties. Lab-on-a-chip devices house microreactors whose electrical properties can change after undertaking chemical reactions. This limits the applications of a sensor that depends on droplet electrical properties.

These feedback control systems for DMF device implement a true/false detection sensor that reports whether a droplet covers an electrode or not based on a calibrated threshold condition. These detection sensors have practical implementation, however, they fail to capture essential droplet dynamic information, particularly in situations where droplets have partial overlap on electrodes. As a result, these feedback controllers are limited by the detection sensor that requires pre-calibration for proper operation and has discrete droplet sensing. They can neither position droplets within the interval of two electrodes nor accurately control the velocity and acceleration of droplets on a DMF device.

Our aim is to develop a droplet position estimator that is independent of droplet composition, thus, requires no calibration. We use electrode capacitance, an inherent electrical property of electrowetting-on-dielectric (EWOD) DMF devices, to determine the position of any droplet composition in the interval of two electrodes. Capacitance is an electrical property that is sensitive to the presence of a droplet and is independent of actuation signal frequency. The estimator uses a dimensionless ratio of electrode capacitances to approximate the droplet position in the interval of two electrodes. Our estimator is independent from the driving signal frequency, droplet composition, and requires minimal computational power. In this research, we implement a capacitance-based position estimator that can continuously track the displacement of a droplet within the interval of two adjacent electrodes. The displacement of a droplet is estimated through a dimensionless ratio of two electrode capacitances. Unlike previous sensing techniques, this sensing technique requires no calibration for any droplet composition. In the following sections, we derive the formulation of the capacitance-based position estimator. The sensor performance is evaluated in 2D and then 3D analytical and numerical simulations of a digital microfluidic device. Finally, simulation observations are verified through experimental measurements.

## 2 Theoretical modelling of capacitance sensor

Fig. 1a shows the equivalent electrical circuit of a single control electrode in a digital microfluidic system with a generic liquid presented here to describe our proposed sensing mechanism.[25–28]

The electrical circuit consists of two parallel circuit networks corresponding to the liquid and ambient region far from the fluid layer interface. The dielectric and hydrophobic layers are modelled as capacitors.[25–28] The ambient medium or filler liquid, such as air, has no free charges and thus is modelled by a capacitor. We generalize the model to include a liquid droplet with an arbitrary conductivity. Hence, the electrical modelling for the liquid droplet is a parallel capacitor and resistor circuit.

The meniscus at the liquid–liquid or liquid–vapour interface slightly distorts the electrical field between the electrodes. However, its effect is negligible for typical DMF systems where the control electrode width to plate gap ratio is large.[26–28] This will be demonstrated by numerical simulations in Section 4.

The electrical reactance of a single control electrode is purely capacitive with a capacitance given by

$$C_{eq} = aA + (b - a)A_L \quad (1)$$

where $a$ is a small constant whose magnitude is inversely proportional to the plate gap because ambient capacitance is the smallest series capacitance, $b$ is a large constant that is inversely proportional to the dielectric layer thickness because the dielectric capacitance is the second smallest series capacitance since the liquid droplet is slightly conductive, $A$ is the area of a square electrode, and $A_L$ is the liquid footprint area over the square electrode.

In DMF systems, droplets are translated in a linear direction towards the adjacent electrode. Consequently, the control electrode capacitance is a function of droplet position because the droplet footprint area directly depends on the droplet position. As a result, the center of the footprint area of a droplet and hence its position can be estimated from the capacitance values of two adjacent electrodes.

Fig. 1b illustrates a droplet with a fixed volume partially overlapping two adjacent control electrodes in a DMF system. A droplet with a circular footprint with a radius of $r$ is centered at a distance of $x_0$ from the center of electrode 1. Electrodes 1 and 2 are squares with a width of $L$, and a separation gap of $L_e$.

At the meridian plane of the droplet, the capacitance per unit length of electrode 1 is given by

 

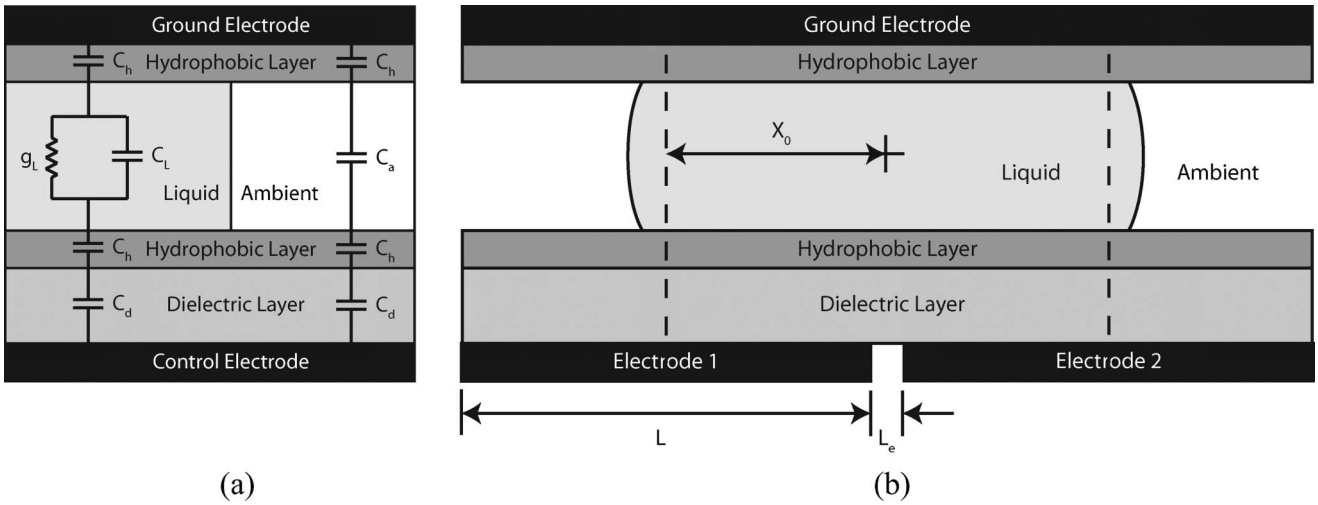


**Fig. 1** (a) Electrical circuit model for a digital microfluidic device with a generic liquid and a non-conductive ambient fluid. (b) Median plane of a liquid droplet positioned between two bottom plate electrodes of a digital microfluidic device.

$$C_1 = aL + (b-a)\left(r + \frac{L}{2} - x_0\right) \tag{2}$$

Similarly, the capacitance of electrode 2 is given by

$$C_2 = aL + (b-a)\left(r - \left(\frac{L}{2} + L_e\right) + x_0\right) \tag{3}$$

Normalizing the capacitance of electrode 2 yields a dimensionless ratio that is a function of droplet center position as

$$\frac{C_2}{C_1 + C_2} = \frac{aL + (b-a)\left(r - \left(\frac{L}{2} + L_e\right) + x_0\right)}{2aL + (b-a)(2r - L_e)} \tag{4}$$

Coefficient $b$ is much larger than coefficient $a$ because the dielectric thickness is much smaller than the plate gap. Therefore,

$$\frac{C_2}{C_1 + C_2} \cong \frac{r - \left(\frac{L}{2} + L_e\right) + x_0}{2r - L_e} \tag{5}$$

Typically in order to successfully actuate a droplet in a DMF device, the droplet footprint area must be slightly larger than a single electrode to overlap the adjacent activated electrode.[15,17] On the other hand, a droplet cannot be much larger than an electrode since there will be a risk of unwanted droplet splitting instead of transportation. Thus, $r \cong \frac{L}{2} + L_e$ is a valid assumption so that eqn (5) can be further simplified as

$$x_0 \cong \frac{C_2}{C_1 + C_2}(L + L_e) \tag{6}$$

As a result, the droplet position estimator is independent of the liquid droplet composition because the droplet position is calculated based on a dimensionless ratio of control electrode capacitances. Hence, this proposed approach significantly facilitates the operation of feedback control DMF devices in the experiments with multiple liquid samples whereas the previous approached reported in the literature require calibrating the device for a liquid sample.[23,24]

## 3 Experimental

### 3.1 Device fabrication

A DMF device was fabricated to verify theoretical observations. The device consists of two overlapping plates separated with a 0.5 mm spacer in between the plates. The bottom plate has a linear array of 2 mm square electrodes spaced 0.2 mm from each other. The bottom plate electrodes were etched onto a 50 mm copper layer over a glass substrate. A thin PDMS layer of 5.9 μm thickness was spin coated over the square electrode followed by a Teflon AF1600 layer of 60 mm. The top plate is an Indium Tin Oxide (ITO) microscope slide coated with 60 mm Teflon AF1600.

### 3.2 Setup

Fig. 2 shows the schematic of the experimental setup in this research. It consists of a computer, capacitance meter, switch box, digital microfluidic device, and microscope camera.

In the experimental setup, a National Instrument PXI system equipped with a digital multimeter (PXI-4072) with a resolution of 0.05 pF was used for capacitance measurements. The switch box is a de-multiplexer with one input and two outputs that is controlled by the computer. Each output from the switch box is connected to each bottom electrode. The top view images are acquired through the microscope camera positioned directly above the device. The microscope is equipped with a 1.4 MPixels camera for a position resolution of 7.3 μm. The microscope scale was calibrated with a slide micrometer.

The experimental process involves droplet generation, droplet deposition, capacitance measurements, and image acquisition. A Gilson micropipette was used to deposit 2.6 μL droplets with a maximum error of ±1%. A droplet was randomly positioned

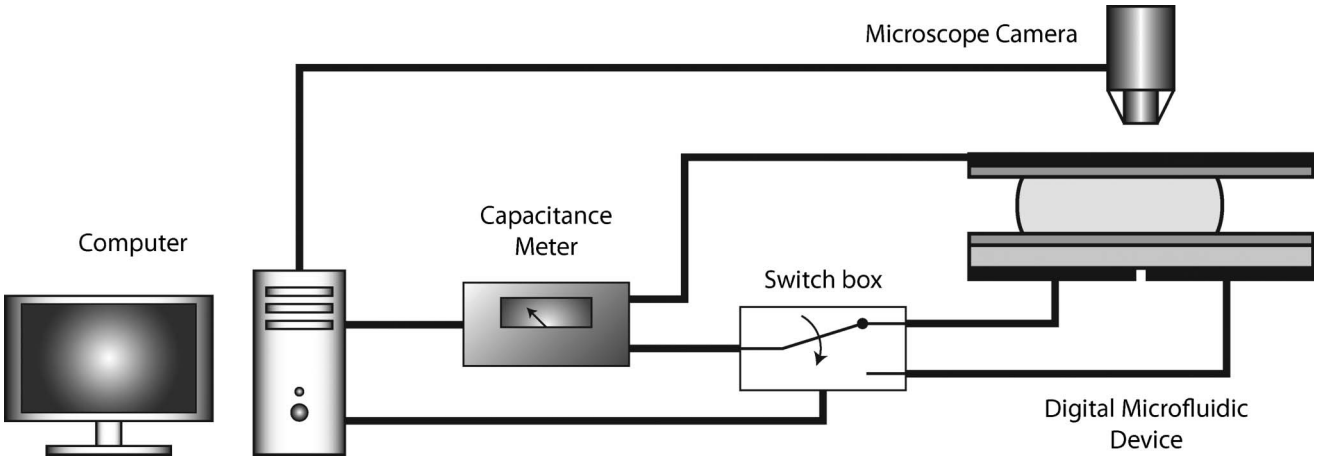


**Fig. 2** Experimental setup schematic for measuring electrode capacitance and droplet position.



between the bottom plate electrodes then capped with the top plate. The random repetitions will prevent biased error in the measurements. Multiple independent capacitance samples were recorded while at the same time capturing top view images of the droplet in a time frame of a few seconds.

## 4 Validation

### 4.1 Theoretical results

The capacitance-based position estimator performance is evaluated with 2D and 3D analytical and numerical simulations of a digital microfluidic device. The analytical simulation ignores electric field fringing but produces a closed-form mathematical function relating electrode capacitances and droplet position. On the other hand, the numerical simulation solves electrostatic equations in a finite element analysis to provide a more realistic estimate of the actual capacitance by taking the fringing electric fields into account. As a result, we expect electrode capacitances computed from numerical simulations to be higher than those computed analytically because of the additional fringe capacitance.

In the 2D analysis, we study a single slice of a droplet to understand the relations between electrode capacitances and droplet position and anticipate sources of errors present in a full 3D analysis.

In this analysis, we model the droplet as having a circular footprint. It is noted that during reversible EWOD actuation experiments we observed that at slow droplet transport speeds the droplet footprint is fairly circular and does not suffer significant footprint elongation. Our experimental observations are consistent with literature results that report a slight droplet elongation.[15] A droplet is positioned at between the centers of two adjacent control electrodes. For each droplet position, the capacitance of each electrode is computed and used to estimate the droplet position with eqn (5). The estimation error is defined as the difference between the estimated position and actual position normalized by the separation distance between the centers of two control electrodes ($L + L_e$).

Simulation parameters match the experimental measurements of the fabricated digital microfluidic device and are summarized in Table 1.

**Table 1** Digital microfluidic device parameters

| Parameter | Value |
|---|---|
| Ambient fluid relative permittivity, $\varepsilon_a$ (air) | 1.0 |
| Control electrode pitch, $L$ | 2.0 mm |
| Control electrode spacing, $L_e$ | 0.2 mm |
| Dielectric layer relative permittivity, $\varepsilon_d$ (PDMS) | 2.65 |
| Dielectric layer thickness, $t_d$ | 5.9 μm |
| Droplet resistivity, $\rho_L$ (DI water) | 18 MΩm |
| Droplet permittivity at 20 °C, $\varepsilon_L$ (DI water) | 80.2 |
| Droplet radius, $r$ | $1.05\frac{L}{2}+L_e$ |
| Plate gap, $D$ | 0.5 mm |

Fig. 3a is a plot of the electrode capacitances at the meridian plane as a function of droplet position. As the droplet travels away from electrode 1 (left electrode), the capacitance of electrode 1 decreases while the capacitance of electrode 2 increases. The flat region on the graph between point (A) and (B) is the result of a larger droplet footprint than the size of the electrodes. At point (C), the capacitances of both adjacent electrodes equalize. It is noted that the numerical capacitances are slightly larger than the analytical capacitances due to a minute additional fringe capacitance.

Fig. 3b plots the normalized error for multiple droplet positions. The maximum estimate error is less than 4% of the maximum intra-electrode droplet displacement. Three types of error affect the position estimator performance. The initial error manifests itself as a position bias and is present when a droplet centered over an electrode partially overlaps the adjacent electrode. The transition error appears as a curved region in the normalized error plot. From point A to B, the capacitance of electrode 1 remains unchanged while the capacitance of electrode 2 increases. The unbalanced rate of change of electrode capacitance results in a nonlinear response of the estimator expressed in eqn (5) leading to the transition error. The third error is the smallest error caused by neglecting coefficient $a$ due to the capacitance of the ambient fluid in eqn (4).

The electrode capacitances for the 3D digital microfluidic simulation are plotted in Fig. 4a. As expected, the capacitance of electrode 1 decreases as the droplet moves towards the adjacent electrode. The electrode capacitance curves have non-linear and linear regions. The non-linear region is caused by the leading and

 

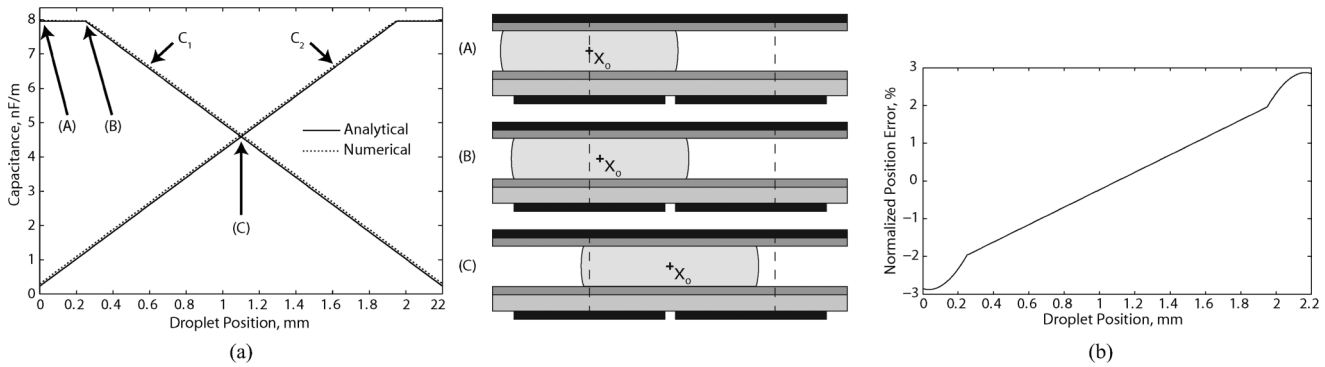


**Fig. 3** (a) 2D Analysis of electrode capacitance at the meridian plane for various droplet positions between the two bottom plate electrodes. (b) Normalized error of the droplet position estimate for various droplet positions between two bottom plate electrodes in a 2D digital microfluidic device.

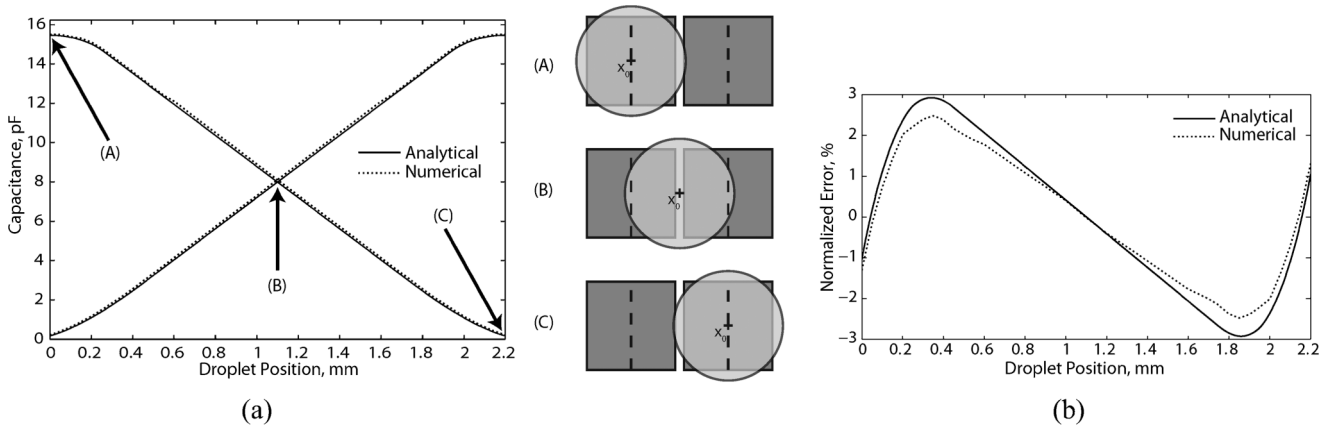


**Fig. 4** (a) 3D Analysis of electrode capacitance for various droplet positions between two bottom plate electrodes. (b) Normalized error of the droplet position estimate for various droplet positions between two bottom plate electrodes in a 3D digital microfluidic device.



trailing droplet edges when they cross over the boundary of a square electrode. The linear region occurs when the leading and tailing droplet edges are fully enclosed within the boundaries of the square electrodes. In both 2D and 3D analysis, analytical and numerical electrode capacitance waveforms have a similar profile; however, numerical capacitance waveforms are slightly higher due to the additional fringe capacitance between the droplet vertical boundaries and the electrodes as mentioned earlier.

Fig. 4b plots the normalized error from the 3D simulations. The normalized error curve resembles a sinusoidal plot. The maximum error is less than 3% of the distance between adjacent bottom plate electrodes and occurs when the droplet is nearly centered over an electrode. As was discussed earlier, the position estimator is susceptible to three error types; initial, transition, and simplification errors. Numerical error results have a higher initial error and lower transitional error when compared to the analytical error values. The higher initial error in the numerical results is attributed to the additional fringe capacitance between the droplet vertical boundaries and the adjacent electrode.

### 4.2 Experimental results

Fig. 5a compares the visual (actual) and capacitive droplet position estimate (estimate) using the line of unity. The visual droplet position was measured from the top-view images taken by the microscope camera. The droplet position estimate was computed using eqn (5). Ideally, position estimates should lie along the unity line. More precisely, the proposed position estimator underestimates the displacement in the first half and overestimates the displacement in the second half of the travel distance. However, the estimates are accurate in the start, middle, and end points which are most likely the points of interest for feedback control of droplet operations.

Another important point is that the induced bias errors will in practice help the controller since the underestimated displacement in the first half will trick the controller into generating a larger control input and further accelerate the droplet in the first half (*i.e.*, reduce the rise time). In contrast, the overestimated displacement will limit the control input and decrease the overshoot in the second half. The estimation error is once again attributed to the three types of errors mentioned before. Experimental and simulation results have similar s-curve profiles.

Fig. 5b plots the normalized error of experimental measurements for random droplet positions. The normalized error plot resembles a sinusoidal plot consistent with simulation results presented earlier. The maximum position estimate error is less than 25% of the distance between the adjacent electrodes. It is noted that the error is significantly less in the two extremes and midpoint where accurate estimates are more critical for feedback.

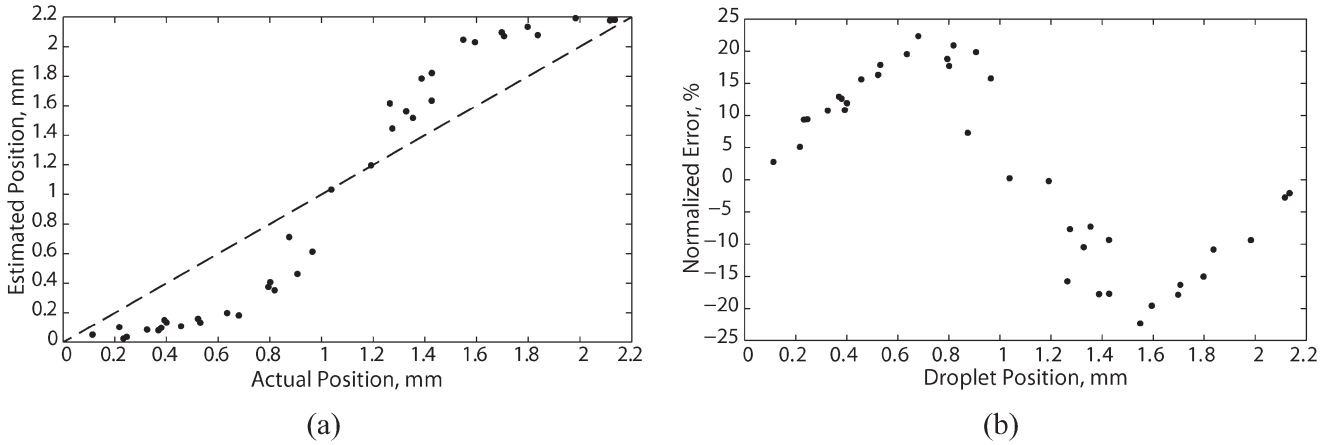


**Fig. 5** (a) Visual and capacitive droplet position plot from experimental measurements. (b) Normalized error plot from experimental measurements of digital microfluidic device.



In these experiments, significant effort was put to minimize the elongation of droplets. Electrode capacitance value measurements were taken under static equilibrium; when the droplet assumes a symmetrical structure with a circular footprint. Top view images of the droplet during the experiments reveal negligible droplet pinning effects even after an incremental actuation. In a parallel on-going research, we were successful in finding a type of actuation signal which minimizes the droplet elongation during droplet movement.

The discrepancies between the model and experimental results are explained by variations in droplet diameter. A parameter sensitivity analysis of the model shows that the diameter droplet footprint has a significant effect on the magnitude and shape of the error curve. A decrease in the droplet radius decreases the initial error while increasing the transient error. As explained earlier, the initial error is a bias error due to the overlap on the adjacent electrode when a droplet is centered over an electrode. The magnitude of the bias error decreases when the droplet diameter is smaller than the pitch of an electrode – the sum of electrode width and inter-electrode gap ($L + L_e$). The transient error arises as the leading and tailing droplet edges cross over the square electrode footprint. When the droplet moves away from the center of an electrode, the overlapped area between the droplet and electrode varies non-linearly. Therefore, smaller droplet diameter increases the magnitude of the transient error producing an s-shape profile. Simulation results with a smaller droplet diameter support this observation. A closer look at top view images of the droplet shows that the outer most droplet diameter was used for simulation results; however, the inner droplet diameter (or circular footprint diameter) is 20% smaller than the outer radius due to the plate gap separation. Reviewing simulation results with a droplet circular footprint to match the inner droplet diameter from the experimental setup yields more convincing results which strongly agreement with experimental data. However, this source of error can be mitigated by constraining the droplet volume such that its footprint slightly overlaps adjacent electrodes when centered over an electrode. This constraint is necessary in practical digital microfluidic devices to facilitate continuous droplet actuation.

Another significant source of error is the effect of droplet misalignment – where the droplet off centered from the meridian plane. In this case, the transition error is increased because the curve length of the leading and tailing droplet edges increases; thus, increasing the position range over which the overlapped area between the droplet and electrode varies non-linearly. In practice, the actuation forces naturally center the droplet on the meridian plane thereby minimizing this source of error. Finally, instrumental errors arising from the droplet dispenser and capacitance meter, though small, have some effect on the outcome of this droplet position estimator.

## 5 Conclusions

In this investigation, we demonstrate a proof of concept through analytical derivation, numerical modeling, and experimental verification that the position of any type of droplet can be estimated with a certain degree of uncertainty in the domain between two electrodes. The droplet position estimator has the capability of monitoring the incremental displacement of droplets in the interval between two adjacent electrodes. This droplet sensing technique is the first of its kind because it incorporates an estimator that approximates the position of a droplet anywhere in between two electrodes. In addition, the droplet position estimate is independent of the composition of the droplet. The fact that this sensing technique performs independent of the electrical properties of the droplet means that sensor implementation requires *no calibration* which is a desirable advantage over previously proposed sensing techniques in particular when dealing with a diverse collection of droplet compositions in a single digital microfluidic device. Although, in our analysis we consider a linear array of electrodes, this droplet sensing approach can readily be applied to a two-dimensional grid of $x$–$y$ electrodes. Specifically, this sensing approach will require considering a group of two adjacent electrodes in either $x$ or $y$ directions for the application in $x$–$y$ electrode grids.

Another distinguishing advantage of this droplet sensing technique is the unprecedented droplet position monitoring capabilities with applications in position feedback control systems for accurately controlling droplet position, velocity and acceleration at sub-electrode resolutions. This sensing approach has the potential to increase the droplet positioning resolution in applications like micro-conveyors whose position

 

resolution and repeatability is limited by the size of the electrodes.

A digital microfluidic system inherently produces a sinusoidal position bias in the state estimator that induces an error in position measurements. However, this sinusoidal bias in the position estimator can benefit the control system to reduce rise time and overshoot. Recently, we rapid-prototyped a programmable feedback controller for EWOD digital microfluidic devices and implemented this sensing approach to demonstrate intra-electrode positioning.

## Acknowledgements

The authors recognize the financial support from the Natural Sciences and Engineering Research Council of Canada (NSERC) and Canada Foundation for Innovation (CFI).

## References

1 J. Berthier, *Microdrops and digital microfluidics*, William Andrew Pub., 2008.
2 I. Barbulovic-Nad, S. H. Au and A. R. Wheeler, *Lab Chip*, 2010, **10**, 1536–1542.
3 I. Barbulovic-Nad, H. Yang, P. S. Park and A. R. Wheeler, *Lab Chip*, 2008, **8**, 519–526.
4 M. J. Jebrail and A. R. Wheeler, *Anal. Chem.*, 2009, **81**, 330–335.
5 Y.-H. Chang, G.-B. Lee, F.-C. Huang, Y.-Y. Chen and J.-L. Lin, *Biomed. Microdevices*, 2006, **8**, 215–225.
6 K. Chakrabarty and F. Su, *Digital microfluidic biochips: synthesis, testing, and reconfiguration techniques*, CRC/Taylor & Francis, 2006.
7 S. K. Cho, H. Moon and C.-J. Kim, *J. Microelectromech. Syst.*, 2003, **12**, 70–80.
8 F. Brochard, *Langmuir*, 1989, **5**, 432–438.
9 M. O. A. Abdelgawad, PhD thesis, University of Toronto, Ontario, Canada, 2009.
10 M. Abdelgawad, P. Park and A. R. Wheeler, *J. Appl. Phys.*, 2009, **105**, 094506.
11 D. Chatterjee, B. Hetayothin, A. R. Wheeler, D. J. King and R. L. Garrell, *Lab Chip*, 2006, **6**, 199–206.
12 J. Zeng and T. Korsmeyer, *Lab Chip*, 2004, **4**, 265–277.
13 J. Lee, *Sens. Actuators, A*, 2002, **95**, 259–268.
14 H. Moon, S. K. Cho, R. L. Garrell and C.-J. C. Kim, *J. Appl. Phys.*, 2002, **92**, 4080–4087.
15 M. G. Pollack, A. D. Shenderov and R. B. Fair, *Lab Chip*, 2002, **2**, 96–101.
16 M. G. Pollack, PhD thesis, Duke University, Durham, North Carolina, USA, 2001.
17 M. G. Pollack, R. B. Fair and A. D. Shenderov, *Appl. Phys. Lett.*, 2000, **77**, 1725–1726.
18 N.-T. Nguyen, K. M. Ng and X. Huang, *Appl. Phys. Lett.*, 2006, **89**, 052509.
19 K. Ichimura, S.-K. Oh and M. Nakagawa, *Science*, 2000, **288**, 1624–1626.
20 A. Wixforth, C. Strobl, C. Gauer, A. Toegl, J. Scriba and Z. v. Guttenberg, *Anal. Bioanal. Chem.*, 2004, **379**, 982–991.
21 E. Yakhshi-Tafti, H. J. Cho and R. Kumar, *Procedia Chem.*, 2009, **1**, 1519–1522.
22 J. Gong and C.-J. C. Kim, *Lab Chip*, 2008, **8**, 898–906.
23 Y.-J. Shin and J.-B. Lee, *Rev. Sci. Instrum.*, 2010, **81**, 014302.
24 S. C. C. Shih, R. Fobel, P. Kumar and A. R. Wheeler, *Lab Chip*, 2011, **11**, 535–540.
25 D. Chatterjee, H. Shepherd and R. L. Garrell, *Lab Chip*, 2009, **9**, 1219–1229.
26 T. B. Jones, J. D. Fowler, Y. S. Chang and C.-J. Kim, *Langmuir*, 2003, **19**, 7646–7651.
27 T. B. Jones, K.-L. Wang and D.-J. Yao, *Langmuir*, 2004, **20**, 2813–2818.
28 T. B. Jones, *J. Micromech. Microeng.*, 2005, **15**, 1184.